Journal of Alloys and Compounds 507 (2010) 77–83

Contents lists available at ScienceDirect

Journal of Alloys and Compounds

journal homepage: www.elsevier.com/locate/jallcom

Synthesis of star-shaped PbS nanocrystals using single-source precursor

Masoud Salavati-Niasari[a,b,*], Azam Sobhani[b], Fatemeh Davar[a,**]

[a] Institute of Nano Science and Nano Technology, University of Kashan, Kashan, P.O. Box 87317-51167, Islamic Republic of Iran
[b] Department of Inorganic Chemistry, Faculty of Chemistry, University of Kashan, Kashan, P.O. Box 87317-51167, Islamic Republic of Iran

ARTICLE INFO

Article history:
Received 6 February 2010
Received in revised form 1 June 2010
Accepted 10 June 2010
Available online 17 June 2010

Keywords:
Lead sulfide
Nanostructures
Hydrothermal
Thermal decomposition
Star-shaped
Optical properties

ABSTRACT

Star-shaped PbS nanostructures were prepared by simple hydrothermal process of [bis(thiosemicarbazide)lead(II)], $[Pb(TSC)_2]Cl_2$ (TSC = thiosemicarbazide), at 150 °C, without any additive. Effect of reaction time on the morphology of the products was investigated. Also PbS nanoparticles was synthesized by thermal decomposition of precursor in the presence of oleylamine and triphenylphosphine as surfactant. In this process, oleylamine was used as both the medium and the stabilizing reagent. Also the novel precursor thermally was treated in solid state reaction in different temperatures, 400, and 500 °C for 5 h. Products were characterized by X-ray diffraction (XRD), scanning electron microscopy (SEM), transmission electron microscopy (TEM), X-ray photoelectron spectroscopy (XPS), photoluminescence spectroscopy (PL) and Fourier transform infrared (FT-IR) spectra. The band gap energy of star-shaped PbS nanostructures has been estimated to be 3.19 eV which shows a large increment compared with that of bulk PbS.

1. Introduction

Lead sulfide (PbS) is an important binary IV–VI semiconductor material which have novel semiconducting and optical properties [1]. It has attracted considerable attention in the field of materials science due to its special small direct band gap energy (0.41 eV, for bulk at room temperature) and a large exciton Bohr radius (18 nm) [2–5]. PbS nanostructures may be one of the most potential candidates for optical devices such as light-emitting diodes and optical switches due to its exceptional third order nonlinear optical properties [6,7].

The single-source molecular precursors to PbS that have been investigated include lead dithiocarbamato complexes [8], lead bis(butylthiolate) compounds [9], lead dichalcogenoimidodiphoshanto complexes [10], etc. Thermal decomposition of these precursors either in refluxing organic solvent [8] or in solid state [9] or in MOCVD [10] can lead to PbS nanocrystallites with different morphologies. Different morphologies can play the roles in the properties. They are nanocrystals [11], nanorods [12,13], nanotubes [12], nanocubes [14], star shapes [15], dendrites [14,16] and flower-like crystals [17] and so on [16,18–23]. Up to date, many methods have been developed to fabricate PbS nanostructures. Among them, the hydrothermal method and thermal decomposition provides a more promising way for the synthesis of crystals due to its low cost, high efficiency and potential for large-scale production. Recently microcrystalline PbS tetrapod like structure has been successfully prepared by a hydrothermal route using $Pb(CH_3COO)_2{\cdot}3H_2O$ and thiourea as reagents and acrylamide (AA) as a surfactant [24].

In our group, for a few years, we have been interested in the synthesis of metal, metal oxide and metal sulfide nanoparticles, using new inorganic precursor, taking profit of the tools of organometallic chemistry [25–31]. At present, the development of organometallic or inorganic compound for preparation of nanoparticles is the major interest [32–36]. Using of the novel compound can be useful and open a new way for preparing nanomaterials to control nanocrystal size, shape and distribution size.

In 1998, Qian et al. [37] reported a one-step route to crystalline PbS by a solvothermal reaction between lead oxalates and elemental sulfur in organic solvents such as ethylenediamine and pyridine. Cheon et al. [38] have synthesized PbS nanocrystals with various rod-based structures including highly faceted star shapes, truncated octahedrons and cubes from the thermal decomposition of a molecular precursor, $Pb(S_2CNEt_2)_2$. Zou et al. [4] have synthesized PbS microcrystals including dendrites, flowers, multipods and cubes from the reaction of dissoluble lead salt (lead nitrate or lead acetate) and thiourea through a simple hydrothermal process. Warner [39] has synthesized PbS nanorods by lead acetate, elemental sulfur and oleic acid as surfactant.

The present work describes the synthesis of PbS nanoparticles using two methods: thermal decomposition and hydrother-

* Corresponding author at: Institute of Nano Science and Nano Technology, University of Kashan, Kashan, P.O. Box. 87317-51167, Islamic Republic of Iran. Tel.: +98 361 5555333; fax: +98 361 5552935.
** Corresponding author. Tel.: +98 361 5555333; fax: +98 361 5552935.
E-mail addresses: salavati@kashanu.ac.ir (M. Salavati-Niasari), davar@kashanu.ac.ir (F. Davar).

0925-8388/$ – see front matter © 2010 Elsevier B.V. All rights reserved.
doi:10.1016/j.jallcom.2010.06.062

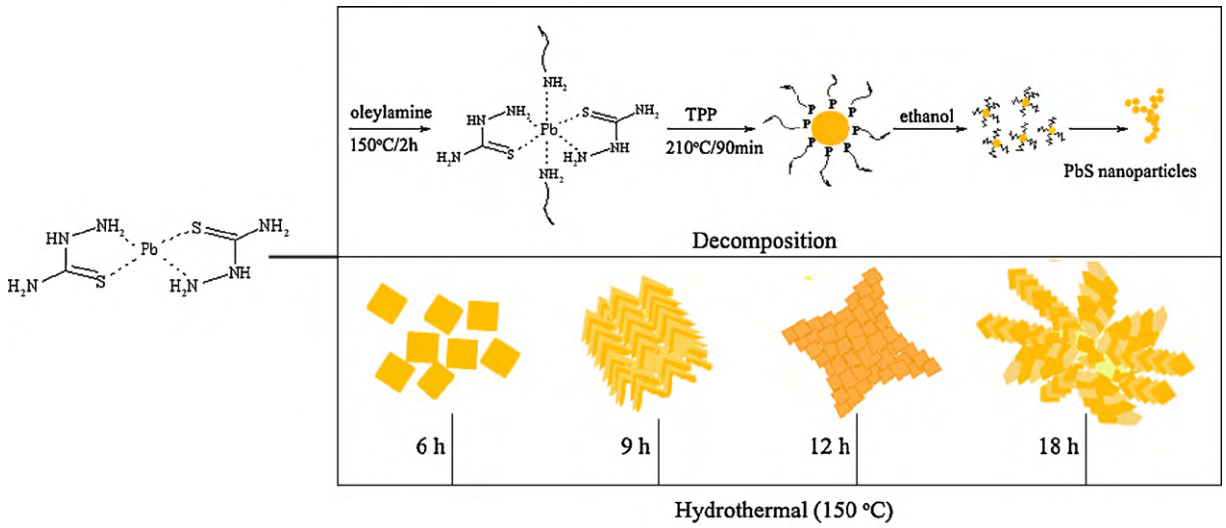

Scheme 1. Schematic diagram illustrating the formation of PbS nanostructures by two methods.

mal route. For these approach [bis(thiosemicarbazide)lead(II)], $[Pb(TSC)_2]Cl_2$ (TSC = thiosemicarbazide) was selected as new precursor. Transition metal complexes containing sulfur–nitrogen chelating agents derived from TSC and their Schiff bases have been extensively studied due to their interesting coordination chemistry [40–42]. The use of TSC complexes of different structures allows controlling the structure of obtained semiconductor materials. To the best of our knowledge the use of $[Pb(TSC)_2]Cl_2$ as precursor in nanoparticles synthesis approach is reported for the first time. In this paper, a simple, green, low cost, and reproducible process for the synthesis of PbS nanocrystals is reported..

2. Experimental

2.1. Materials and physical measurements

All the chemicals were of analytical grade and were used and received without further purification. XRD patterns were recorded by a Rigaku D-max C III, X-ray diffractometer using Ni-filtered Cu Kα radiation. Elemental analyses were obtained from Carlo ERBA Model EA 1108 analyzer. The surface of the lead sulfide compound was characterized by X-ray photoelectron spectroscopy (XPS) ESCA-3000 electron spectrometer with non-monochromatic Mg K_α radiation was used to excite the photoelectrons. Scanning electron microscopy (SEM) images were obtained on Philips XL-30ESEM equipped with an energy dispersive X-ray spectroscopy. Transmission electron microscopy (TEM) images were obtained on a Philips EM208 transmission electron microscope with an accelerating voltage of 100 kV. Fourier transform infrared (FT-IR) spectra were recorded on Shimadzu Varian 4300 spectrophotometer in KBr pellets. Room temperature photoluminescence (PL) was studied on an F-4500 fluorescence spectrophotometer.

2.2. Synthesis of $[Pb(TSC)_2]Cl_2$ complex

Lead(II) chloride, 2 mmol, was dissolved in 20 ml distilled water, a solution of thiosemicarbazide ($H_2NNHCSNH_2$), 4 mmol, dissolved in 50 ml of distilled water containing 37% hydrochloric acid was dropwise added to the above solution under magnetic stirring. After addition of all reagents, the mixture was refluxed for about 6 h. After evaporation of the solution; a white crystalline solid was recovered. It was filtered, washed with distilled water and ethanol and dried. We suppose that thiosemicarbazide is coordinated to cadmium ion as bidentate cyclic ligand through the S atom and the terminal N atom of the hydrazine fragment. IR (KBr) ν_{max} (cm^{-1}): 3264 $\nu_{as}(NH_2)$, 3231 $\nu_s(NH_2)$, 3174 ν(NH), 1148 ν(C–N), 789 ν(C=S), 410 ν(M–S), 364 ν(M–N). Anal. Calcd. (%) for $[Pb(TSC)_2]Cl_2$: C, 5.22; H, 2.19; N, 18.26; S, 13.93; Pb, 45.01. Found (%): C, 5.14; H, 2.32; N, 18.43; S, 13.81; Pb, 45.06 [42–44].

2.3. Preparation of PbS nanoparticles

In the current synthetic procedure that has been shown in Scheme 1, first, 0.6 g $[Pb(TSC)_2]Cl_2$ and 5 ml oleylamine loaded in a 50 ml two-neck distillation were heated up to 150 °C for 120 min and a light yellow solution was generated with the gradual dissolution of precursor complex $[Cd(TSC)_2]Cl_2$. Then, 5 g of triphenylphosphine (TPP) was dissolved in the mixture. The solution was aged at 210 °C for 90 min. The color of the solution changed from yellow to orange, indicating that colloidal nanoparticles were generated. The thermal decomposition of the thiosemicarbazide complex at 210 °C led to a formation of PbS nanoparticles. By adding excess ethanol to the solution, the nanoparticles were precipitated. The yellow precipitate was collected via centrifugation after 15 min of stirring. The nanoparticles could easily be re-dispersed in nonpolar organic solvents, such as hexane or toluene. This synthetic procedure is a modified version of the method developed by Hyeon and co-workers for the synthesis of nanocrystals of metals that employs the thermal decomposition of transition metal complexes [45].

2.4. Preparation of star-shaped PbS nanocrystals

Star-shaped PbS nanocrystals were synthesized following this procedure: 0.8 g of the $[Pb(TSC)_2]Cl_2$ dissolved in 50 ml of distilled water, was put into a Teflon-lined stainless steel autoclave of 100 ml capacity. The autoclave was sealed and maintained at 150 °C for 12 h, then allowed to cool to room temperature naturally. The yellow solid formed was separated by centrifugation and re-dissolved in toluene for further analysis. The nanoflowers dried in vacuum at 50 °C for 2 h. In the current synthetic procedure that has been shown in Scheme 1, the yield of the overall synthesis was 76% based on the amount of $[Pb(TSC)_2]Cl_2$.

3. Results and discussion

Fig. 1a–c shows the XRD patterns of the precursor of $[Pb(TSC)_2]Cl_2$, PbS nanoparticles and star-shaped PbS nanocrystals. In Fig. 1a all the reflections in the pattern could be indexed on the basis of an monoclinic cell reported for $[Pb(TSC)_2]Cl_2$, indicating the pure $[Pb(TSC)_2]Cl_2$ precursor was obtained. XRD of the PbS nanocrystals is shown in Fig. 1b. The XRD pattern reveals the cubic rock-salt structure of PbS without obvious characteristic reflection peaks from other impurities according to JCPDS No. 78-1898 with the lattice parameter $a = 5.918$ Å. The broadening peaks caused by the small size of PbS nanocrystals. The size of PbS nanocrystals calculated from the Scherrer formula is 35 nm. As shown in Fig. 1c, all peaks can be readily indexed as face-centered-cubic PbS structure with a lattice constant $a = 5.942$ Å in agreement with the literature value (JCPDS No. 77-0244, $a = 5.934$ Å). The strong and broaden peaks show that the material has good crystallization and small size. No impurity was found in Fig. 1c, implying the product is pure. Compared to the standard card, the strong (2 0 0) peak reveals the [1 0 0] oriented growth of the star-shaped PbS crystals.

Energy dispersive X-ray spectroscopy (EDX), further confirmed that the nanocrystals were composed of PbS. The EDX of the typical product PbS nanoparticles is shown in Fig. 2. Peaks associated with Pb and S are clearly observed and provide strong evidence that the nanocrystals are composed of PbS [4]. The peaks associated with copper, oxygen, and carbon in the EDX spectrum come from the

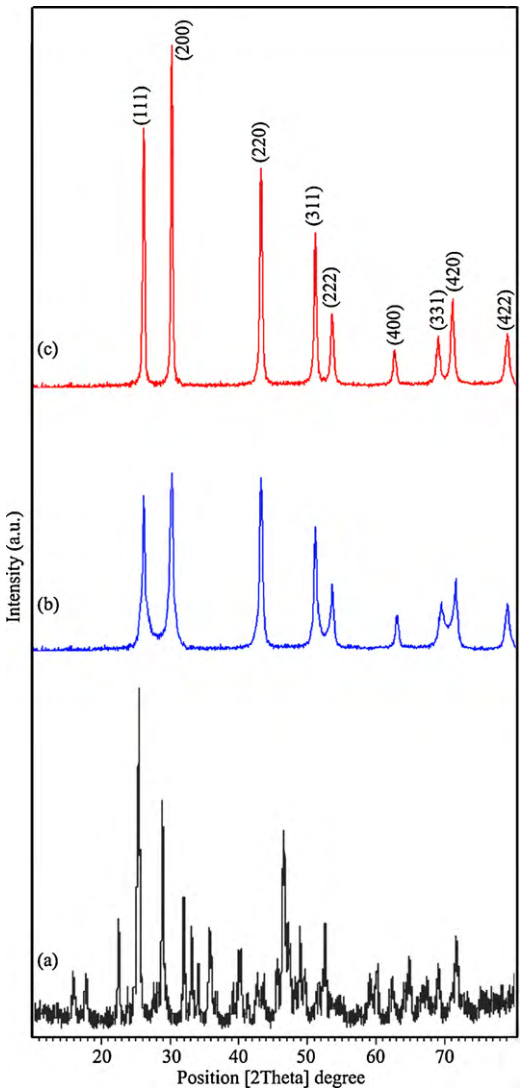

Fig. 1. XRD patterns of (a) $[Pb(TSC)_2]Cl_2$, (b) PbS nanoparticles (sample no. 1) and (c) star-shaped PbS nanocrystals (sample no. 2).

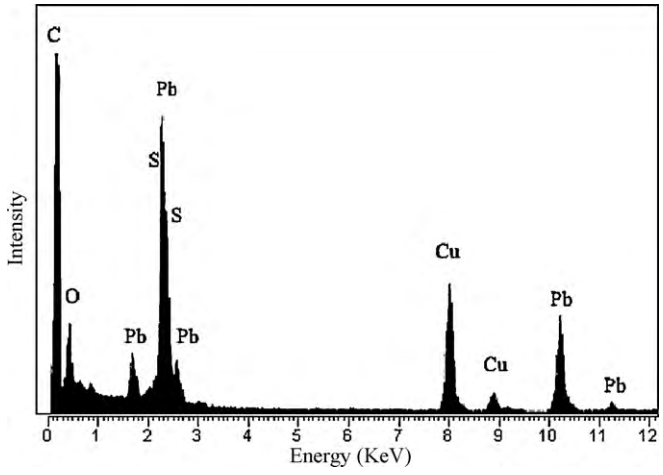

Fig. 2. Energy dispersive X-ray spectrum taken from an as-synthesized PbS nanocrystals (sample no. 2).

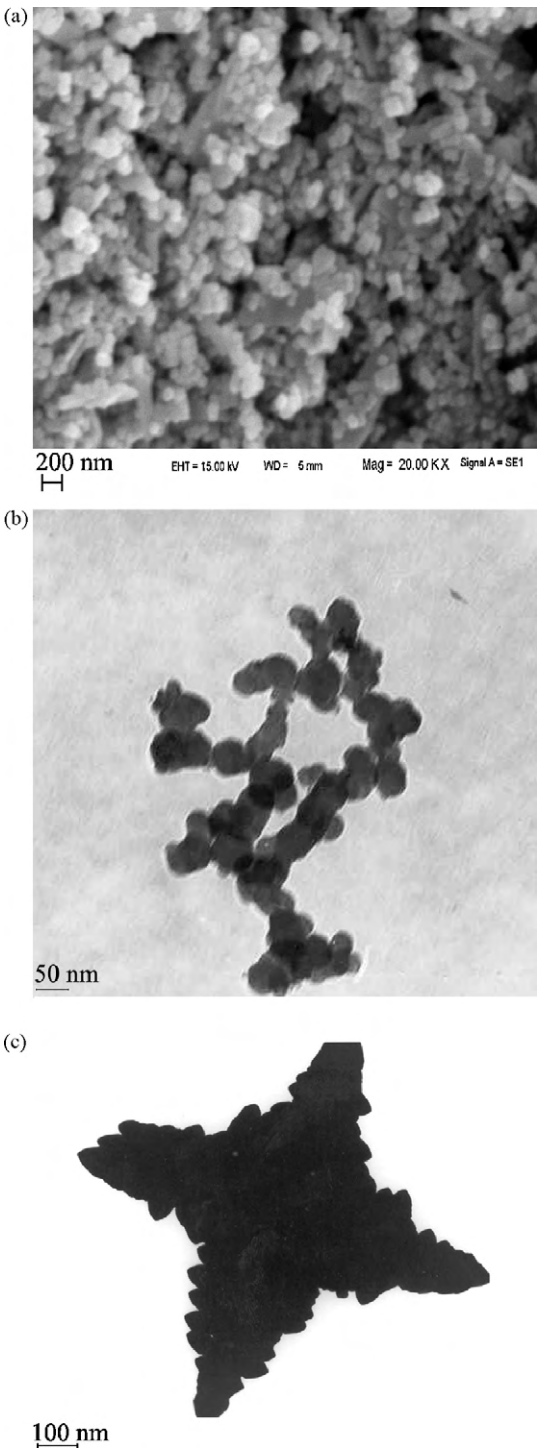

Fig. 3. (a and b) SEM and TEM images of sample no. 1 and (c) TEM image of sample no. 2.

grids used for TEM analysis. The EDX results of other products are similar.

The morphology and structure of the as-prepared PbS were investigated by SEM and TEM images. Fig. 3a shows the SEM image of sample no. 1. The SEM analysis images (Fig. 3a) show that the morphology of powder is granular. It can be clearly seen that there exists a great deal of uniform PbS spherical nanoparticles. Fig. 3b shows TEM image of PbS nanocrystals (sample no. 1). The shape of the sample is close to regular spherical. More interesting, the nanoparticles self-assemble to Y-shaped flakes as marked with cir-

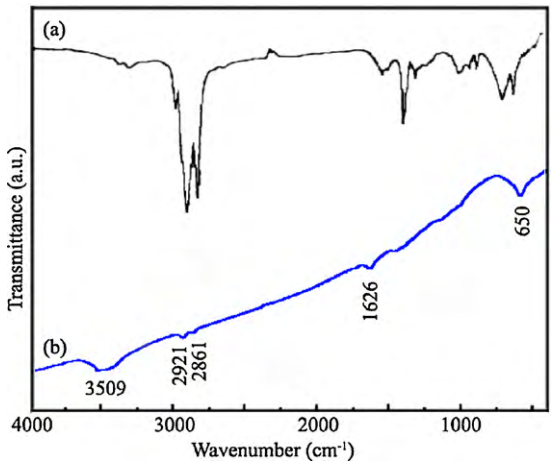

Fig. 4. FT-IR spectra of (a) oleylamine and (b) sample no. 1.

cles. The average size observed from TEM was in good agreement with the value calculated 30–40 from Scherrer formula. Fig. 3c presents a typical TEM image of a star-shaped PbS crystal, sample no. 2, with its four arms standing on the copper grid. In fact that, further observation based on the Fig. 3c shows the stars are composed of small crystals with average diameter of about 30 nm that collected and formed a big star-like structures. This novel hierarchical, four-arm star-shaped PbS crystals is obviously different from the six-arm, eight-arm and star-shaped PbS crystals obtained via simple solution route and polymer-surfactant-assisted route [46–48]. To the best of our knowledge, this is the first report on synthesis of such micrometer-sized three-dimensional (3D) star-like PbS particles with four symmetric arms via hydrothermal method free template and sulfur source. The XRD results (as shown in Fig. 1c) indicated that the as-synthesized PbS are well crystallized due to strong sharp diffraction peaks.

FT-IR spectroscopy is a useful tool to realize the functional group of any organic molecule (Fig. 4a and b). The presence of oleylamine group on PbS nanoparticles (Fig. 4b) is indicated by two peaks at 2921 and 2861 cm^{-1} which represent the C–H stretching modes of the oleylamine carbon chain and matches with oleylamine spectrum. This indicates that small amount of oleylamine bind on the surface through the unpaired electron couple of the amine group [49]. The broad peak at ca. 3509 cm^{-1} and the weak peak at 1626 cm^{-1} are assigned to the stretching and bending vibration of absorption water on surface of nanocrystals, respectively. More careful observation shows that there is a peak at 650 cm^{-1} corresponding to PbS bonds [50].

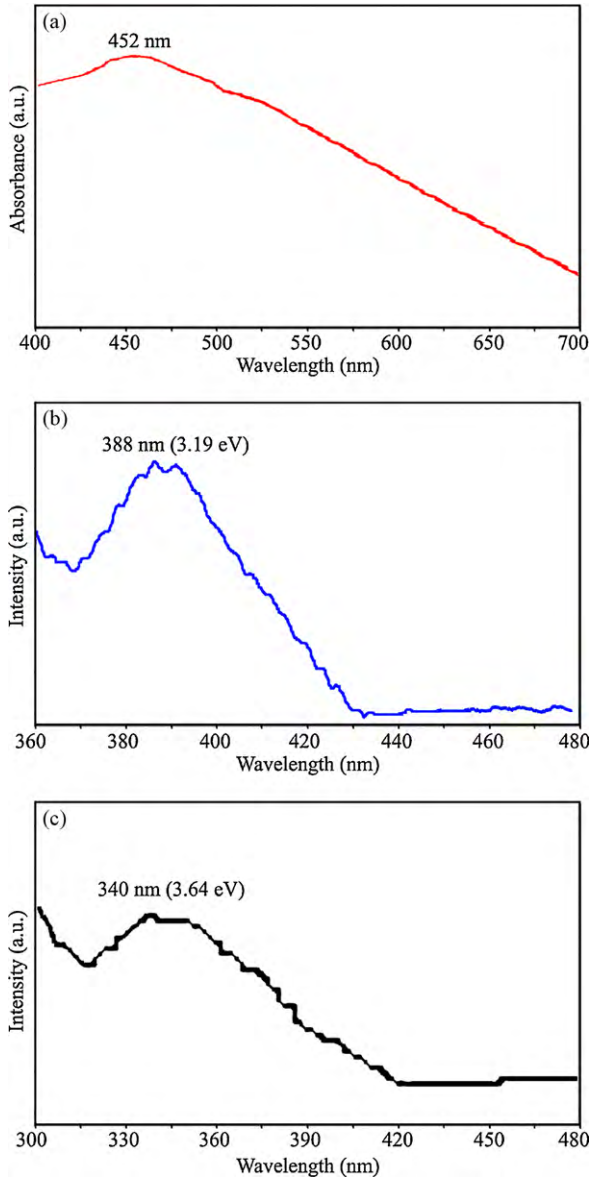

Fig. 6. The UV–vis absorption spectrum of (a) sample no. 2 and (b and c) PL spectra of sample no. 2 and sample no. 1, respectively.

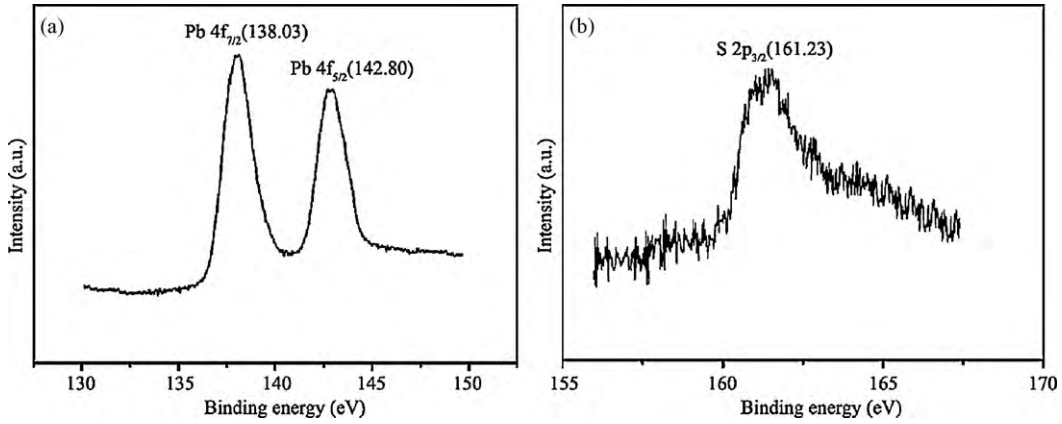

Fig. 5. XPS spectra of the as-synthesized PbS nanocrystals (sample no. 2): (a) Pb 4f core level and (b) S 2p core level.

Table 1
Preparation of PbS under different conditions.

Sample no.	Method	Capping agent	T (°C)	Time	Product
1	Thermal decomposition	Oleylamine + TPP	260	90 min	PbS nanoparticles (30–40 nm) (Fig. 3b)
2	Hydrothermal		150	12 h	Star-shaped PbS nanocrystals (Fig. 3c)
3	Solid state reaction		400	5 h	PbS nanoparticles (Fig. 7a)
4	Solid state reaction	–	500	5 h	PbS nanoparticles with large size (Fig. 7b)
5	Hydrothermal	–	150	6 h	PbS nanocubic (Fig. 8a)
6	Hydrothermal	–	150	9 h	Fish bone like PbS (Fig. 8b)
7	Hydrothermal		150	18 h	Star-shaped PbS (Fig. 8b)

Fig. 5 shows the XPS spectra of the sample no. 2, star-shaped PbS nanocrystals. The spectra confirmed the formation of PbS crystals with molar ratios of Pb:S of 1.00: 1.05. The XPS of Pb 4f region and S 2p region are shown in Fig. 5a and b. The values of the binding energy were calibrated using C 1 s peak (284.6 eV) as the internal standard. The peaks at 138.03 and 142.80 eV correspond to Pb $4f_{7/2}$ and Pb $4f_{5/2}$ and the peak at 161.23 eV correspond to the S 2p transition, respectively. The binding energies for Pb and S are in agreement with the literature values for PbS [4] and no peaks apart from Pb, S, C and O were detected.

Besides the size of the star-shaped PbS, sample no. 2, is considerably larger than the exciton Bohr radius (18 nm). Considering the fact, quantum-confinement effects seem inexistent [51]. But quantum-confinement effects occur near the peak edge of the tips, which are smaller than the Bohr radius of PbS, since the optical properties of non-spherical nanocrystals are controlled by the lowest dimension of nanocrystals [52]. For the star-shaped PbS with thin tips exhibiting quantum confinement, it could be observed that the band gap energy increases from the inner thicker part to the tip edge of the crystals due to position-dependent quantum-size effects [53]. Fig. 6a shows the UV–vis absorption spectrum of the as-synthesized PbS. In Fig. 6a a broad absorption peak around approximate 452 nm (2.74 eV) can be observed, which is similar to Jiao's report [51]. This result indicates a large blue shift from the bulk PbS (3020 nm) due to quantum-confinement effects, which may be attributed to the relatively large and polyhedron faceted nanoparticles with regular shapes and thin tips. Using the result of comparison between experimental and theoretical data for PbS dots, which has reported by Baskoutas et al. [54], the tip diameter of star-shaped PbS crystal (for the UV–vis at 2.74 eV) was estimated about 1 nm.

PbS nanocrytallites have a unique property of luminescence characteristics, whose specific emission wavelengths mainly depend on the nature of the semiconductors, the physical dimensions and the chemical environments, bringing on great application potentialities in the fields of optoelectronic (light-emitting) devices and biosensors. Fig. 6b and c shows the photoluminescence (PL) emission spectrum of the as-synthesized samples dissolved in chloroform. Fig. 6b shows the PL spectrum of sample no. 2. The sample kept at room temperature was excited with excitation wavelength 320 nm using a xenon lamp. The band gap energy of sample no. 2 has been estimated to be 3.19 eV which shows a large increment compared with that of bulk PbS (0.41 eV) [55,24]. Cao et al. [56] also observed a large blue shift of the absorption edge for their synthesized PbS nanocubes. The quantum confinement may occur near the tip edge of the PbS tetrapods, which are smaller or comparable to PbS Bohr radius. Chattopadhyay and co-workers [24] reported a blue shift for their prepared tetrapod PbS. They believed that the PL peak around 440 nm wavelength may be ascribed due to the transition of electrons from the conduction band edge to holes trapped at surface states located within the band gap energy. Fig. 6c is the PL excitation spectrum of the PbS nanoparticles in sample no. 1. Under PL excitation at 320 nm, the PbS nanoparticles emit blue light as 340 nm (corresponding to 3.64 eV).

Besides the main route explained so far, another method was examined to investigate the morphology of products, if any, and to make a comparison between them. Solid state reaction which is a thermal method and starts with solid precursor extensively has been employed to prepare various nanoparticles. In this method, the precursor is heated up to a specific temperature for a given time without presence of any surfactants or solvents. As shown in Table 1, three two different approaches including thermal decom-

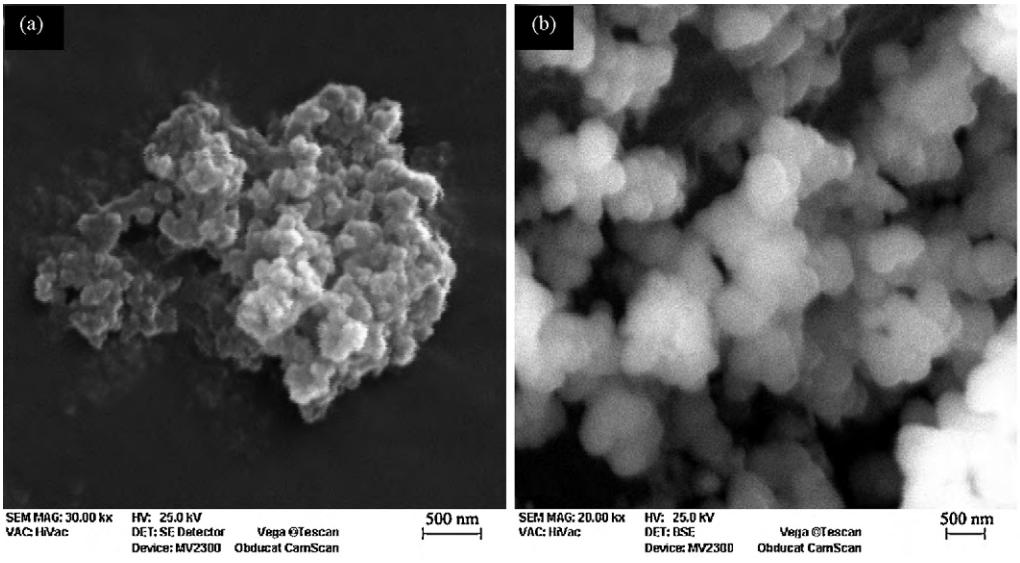

Fig. 7. SEM images of the PbS products obtained via solid state reaction at reaction temperature: (a) 400 °C (sample no. 3) and (c) 500 °C (sample no. 4).

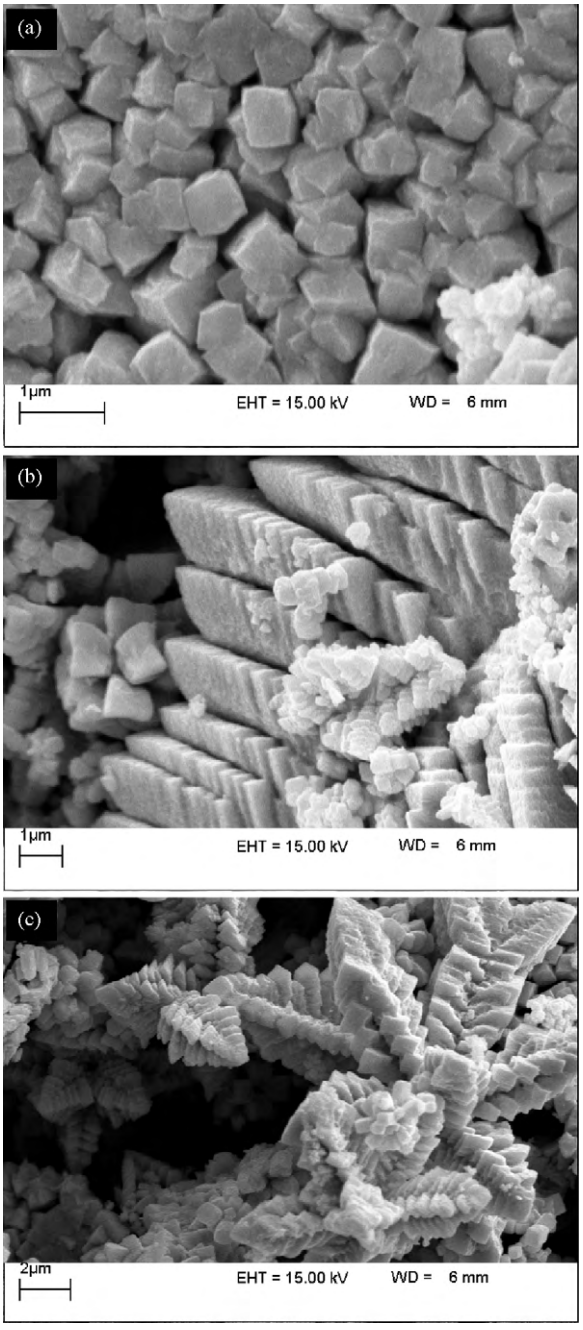

Fig. 8. SEM images of the PbS products obtained via hydrothermal method for different reaction times: (a) 6 h (sample no. 5), (b) 9 h (sample no. 6) and (c) 18 h (sample no. 7).

position, hydrothermal and solid state reaction were examined. To investigate the importance of surfactant role in temperature decrease, in the third approach $[Pb(TSC)_2]Cl_2$ were calcined at 400 and 500 °C for 5 h in surfactant free conditions (sample no. 3 and sample no. 4). A schematic view of third approach and morphology of the products is shown by SEM images in Fig. 7. It is clear that in 400 °C nanoparticles with the smallest size are obtained (Fig. 7a). As the temperature is increased, the small nanoparticles grow at 500 °C (Fig. 7b). Considering different conditions employed to prepare these samples, it is obvious that using oleylamine and TPP as capping agent decreases the reaction temperature and is preferred for PbS nanoparticle synthesis.

The effects of reaction time on hydrothermal method on the morphology and shape of PbS powders are shown in Fig. 8. For this propose reaction were carried out with different reaction times. When the reaction was carried out for 12 h, the star-shape nanostructures were observed (Fig. 3c). Only cubic PbS crystals were obtained when the reaction time was decreased to 6 h (Fig. 8a). When the reaction time was prolonged to 9 h the quasi-cubic structures converted to fish bone like (Fig. 8b). With increasing the reaction time to 18 h the star-shaped nanostructures are bigger (Fig. 8c). This type of crystal growth is consistent with Oswald ripening.

According to the previous report [57] the formation of PbS star-like nanostructure can be explained as follow: prior to the hydrothermal process, the dissociation of S^{2-} from $[Pb(TSC)_2]Cl_2$ is significantly slow, and the formation of complexed PbS clusters, $(PbS)_m$, is fairly limited. Meanwhile, during the hydrothermal process, the formation of $(PbS)_m$, is remarkable due to the enhanced dissociation S^{2-} from the precursor $[Pb(TSC)_2]Cl_2$ at high temperature and pressure. In this case, it is invisible that the complexed PbS clusters aggregate somewhere, because they are formed at a high rate. Therefore, PbS star-like nanostructure were formed in this sample. Therefore, during the hydrothermal process, the formation of PbS proceeds along specific directions. Moreover, in our work, it was found that the quasi-cubic PbS nanoparticles were formed by hydrothermal method for less than 9 h. Therefore, time of reaction is one key factor for the hydrothermal formation of star-shaped PbS crystals. The exact mechanism for the formation of star-shaped PbS crystals in hydrothermal process is still under investigation.

4. Conclusion

PbS nanostructures were obtained from [bis(thiosemicarbazide)lead(II)], as precursor, using two simple method, hydrothermal and thermal decomposition process. These methods have some advantages such as simple process, low cost and easiness to obtain high purity products; hence it is quite promising and facile route for industrial applications. PbS nanoparticles with size about 30–40 nm was prepared via a simple approach in oleylamine as organic solvent via decomposition of a single precursor. Also star-shaped PbS was synthesized via hydrothermal method without any surfactant. It may also be extended to the preparation of some other sulfide nanostructures. The effect of reaction time, which is known as the key parameter on the morphology and particle size of products was investigated.

Acknowledgment

The authors are grateful to University of Kashan for their unending effort to provide financial support to undertake this work.

References

[1] A.M. Qin, Y.P. Fang, W.X. Zhao, H.Q. Liu, C.Y. Su, J. Cryst. Growth 283 (2005) 230–241.
[2] L. Xu, W. Zhang, Y. Ding, W. Yu, J. Xing, F. Li, Y.T. Qian, J. Cryst. Growth 273 (2004) 213–219.
[3] Y.C. Zhang, T. Qiao, X.Y. Hu, G.Y. Wang, X. Wu, J. Cryst. Growth 277 (2005) 518–523.
[4] S. Wang, A. Pan, H. Yin, Y. He, Y. Lei, Z. Xu, B. Zou, Mater. Lett. 60 (2006) 1242–1246.
[5] S. Zhou, Y. Feng, L. Zhang, J. Mater. Res. 18 (2003) 1188–1191.
[6] V.L. Colvin, M.C. Schlamp, A.P. Alivisatos, Nature 370 (1994) 354–357.
[7] A. Dementjev, V. Gulbinas, L. Valkunas, Phys. Status Solidi B 241 (2004) 945–951.
[8] P. O'Brien, J. Mater. Chem. 7 (1997) 1011–1016.
[9] G. Kraüter, P. Favreau, W.S. Rees, Chem. Mater. 6 (1994) 543–549.
[10] M. Afzaal, K. Ellwood, N.L. Pickett, J. Mater. Chem. 14 (2004) 1310–1315.
[11] U.K. Gautam, R. Seshadri, Mater. Res. Bull. 39 (2004) 669–676.
[12] S.F. Wang, F. Gu, M.K. Lü, G.J. Zhou, A.Y. Zhang, J. Cryst. Growth 289 (2006) 621–625.
[13] T. Saraidarov, R. Reisfeld, A. Sashchiuk, E. Lifshitz, Physica E 37 (2007) 173–177.
[14] W. Zhang, Q. Yang, L. Xu, W. Yu, Y.T. Qian, Mater. Lett. 59 (2005) 3383–3388.

[15] G. Zhou, M. Lü, Z. Xiu, S. Wang, H. Zhang, Y. Zhou, S. Wang, J. Phys. Chem. B 110 (2006) 6543–6548.
[16] Z. Zhang, S.H. Lee, J.J. Vittal, W.S. Chin, J. Phys. Chem. B 110 (2006) 6649–6654.
[17] Y. Ni, F. Wang, H. Liu, G. Yin, J. Hong, X. Ma, Z. Xu, J. Cryst. Growth 262 (2004) 399–402.
[18] H. Zhang, M. Zuo, S. Tan, G.P. Li, S.Y. Zhang, Nanotechnology 17 (2006) 2931–2936.
[19] D.B. Kuang, A.W. Xu, Y.P. Fang, H.Q. Liu, C. Frommen, D. Fenske, Adv. Mater. 15 (2003) 1747–1750.
[20] M.-S. Mo, M.-W. Shao, H.-M. Hu, L. Yang, W.-C. Yu, Y.-T. Qian, J. Cryst. Growth 244 (2002) 364–368.
[21] Q. Lu, F. Gao, S. Komarneni, Nanotechnology 17 (2006) 2574–2580.
[22] C. Zhang, Z.H. Kang, E.H. Shen, E.B. Wang, L. Gao, F. Luo, C.G. Tian, C.L. Wang, Y. Lan, J. Phys. Chem. B 110 (2006) 184–189.
[23] A.L.P. Cornacchio, N.D. Jones, J. Mater. Chem. 16 (2006) 1171–1177.
[24] S. Jana, S. Goswami, S. Nandy, K.K. Chattopadhyay, J. Alloys Compd. 481 (2009) 806–810.
[25] M. Salavati-Niasari, F. Davar, Mater. Lett. 63 (2009) 441–443.
[26] F. Davar, M. Salavati-Niasari, Z. Fereshteh, J. Alloys Compd. 496 (2010) 638–643.
[27] F. Davar, Z. Fereshteh, M. Salavati-Niasari, J. Alloys Compd. 476 (2009) 797–801.
[28] M. Salavati-Niasari, M.R. Loghman-Estarki, F. Davar, J. Alloys Compd. 145 (2009) 346–356.
[29] M. Salavati-Niasari, F. Davar, M.R. Loghman-Estarki, J. Alloys Compd. 494 (2010) 199–204.
[30] M. Salavati-Niasari, N. Mir, F. Davar, J. Alloys Compd. 476 (2009) 908–912.
[31] M. Salavati-Niasari, N. Mir, F. Davar, J. Alloys Compd. 493 (2010) 163–168.
[32] N. Bouropoulos, G.C. Psarras, N. Moustakas, A. Chrissanthopoulos, S. Baskoutas, Phys. Status Solidi A 205 (2008) 2033–2037.
[33] S. Baskoutas, P. Giabouranis, S.N. Yannopoulos, V. Dracopoulos, L. Toth, A. Chrissanthopoulos, N. Bouropoulos, Thin Solid Films 515 (2007) 8461–8464.
[34] M. Salavati-Niasari, D. Ghanbari, F. Davar, J. Alloys Compd. 488 (2009) 442–447.
[35] M. Salavati-Niasari, F. Davar, M.R. Loghman-Estarki, J. Alloys Compd. 481 (2009) 776–780.
[36] F. Mohandes, F. Davar, M. Salavati-Niasari, J. Magn. Magn. Mater. 322 (2010) 872–877.
[37] S.-H. Yu, J. Yang, Y.-S. Wu, Z.-H. Han, J. Lu, Y. Xie, Y.T. Qian, J. Mater. Chem. 8 (1998) 1949–1951.
[38] S.M. Lee, Y.W. Jun, S.N. Cho, J.W. Cheon, J. Am. Chem. Soc. 124 (2002) 11244–11245.
[39] J.H. Warner, Adv. Mater. 20 (2008) 784–787.
[40] A.A. El-Asmy, O.A. El-Gammal, H.S. Saleh, Spectrochim. Acta A 71 (2008) 39–44.
[41] R. Sankar, C.M. Raghavan, R.M. Kumar, R. Jayavel, J. Cryst. Growth 305 (2007) 156–161.
[42] R.M. El-Shazly, G.A.A. Al-Hazmi, Spectrochim. Acta A 71 (2009) 1885–1890.
[43] E. Larsen, P. Trinderup, Acta Chem. Scand. A 29 (1975) 481–483.
[44] P.S. Nair, G.D. Scholes, J. Mater. Chem. 16 (2006) 467–471.
[45] J. Park, E. Kang, S.U. Son, H.M. Park, M.K. Lee, J. Kim, K.W. Kim, H. Noh, J. Park, C.J. Bae, J.-H. Park, T. Hyeon, Adv. Mater. 17 (2005) 429–434.
[46] Y. Ma, L. Qi, J. Ma, H. Cheng, Cryst. Growth Des. 4 (2004) 351–354.
[47] Y. Ni, H. Liu, F. Wang, Y. Liang, J. Hong, X. Ma, Z. Xu, Cryst. Growth Des. 4 (2004) 759–764.
[48] X. Zhao, J. Yu, B. Cheng, Mater. Chem. Phys. 101 (2007) 379–382.
[49] B.A. Korgel, S. Fullam, S. Connolly, D. Fitzmaurics, J. Phys. Chem. B 102 (1998) 8379–8388.
[50] Z. Qiao, Y. Xie, Y. Zhu, Y.T. Qian, J. Mater. Chem. 9 (1999) 1001–1002.
[51] J. Jiao, X. Liu, W. Gao, C. Wang, H. Feng, X. Zhao, L. Chen, Solid State Sci. 11 (2009) 976–981.
[52] K.K. Nanda, S.N. Dahu, Adv. Mater. 13 (2001) 280–283.
[53] Y.W. Jun, J.H. Lee, J.S. Choi, J. Cheon, J. Phys. Chem. B 109 (2005) 14795–14806.
[54] S. Baskoutas, A.F. Terzis, W. Schommers, J. Comput. Theor. Nanosci. 3 (2006) 269–271.
[55] M.F. Acosta, M.S. Lerma, H.A. Chavez, F.F.C. Barraza, R.R. Bon, Solid State Commun. 128 (2003) 407–411.
[56] H. Cao, G. Wang, S. Zhang, X. Zhang, Nanotechnology 17 (2006) 3280–3287.
[57] Y. Ji, X. Ma, H. Zhang, J. Xu, D. Yang., Phys. Condens. Matter 15 (2003) 7611–7615.